J|A|C|S
ARTICLES

Published on Web 05/06/2010

Self-Assembly, Dynamics, and Phase Transformation Kinetics of Donor−Acceptor Substituted Perylene Derivatives

Nikos Tasios,† Christos Grigoriadis,† Michael Ryan Hansen,‡
Henrike Wonneberger,‡ Chen Li,‡ Hans W. Spiess,‡ Klaus Müllen,‡,* and
George Floudas†,*

Department of Physics, University of Ioannina, 451 10 Ioannina, Greece and Foundation for Research and Technology-Hellas (FORTH-BRI), and Max-Planck Institute for Polymer Research, 55128 Mainz, Germany

Received March 18, 2010; E-mail: gfloudas@cc.uoi.gr; muellen@mpip-mainz.mpg.de

Abstract: The role of alkyl chain substitution on the phase formation and core dynamics is studied in a series of diphenylamine functionalized perylenemonoimides (PMIs), by X-ray scattering, calorimetry and site-specific solid-state NMR techniques. In addition, the strong dipole associated with the donor−acceptor character of the molecules allow an investigation of the dynamics with dielectric spectroscopy. The self-assembly revealed an ordered phase only in PMIs with branched alkyl chains. This phase comprises a helical stacking of molecules with a molecular twist angle of 60°. Results from solid-state NMR further pointed out the importance of intramolecular hydrogen bonding in stabilizing the intracolumnar packing within the ordered phase. Moreover, the core dynamics are frozen as revealed by the value of the dynamic order parameters and the reduced strength of dipolar relaxation. The kinetics of phase transformation from the isotropic to the ordered phase proceeds via a nucleation and growth mechanism, and the rates are dominated by the nucleation barrier. Within the isotropic phase the core dynamics display strong temperature dependence with rates that depend on the number of methylene units in the alkyl chains.

Introduction

Discotic liquid crystals (DLCs), consisting of rigid disk-shaped aromatic cores and disordered alkyl substituents, tend to organize into columnar supramolecular structures.[1] Their self-assembly is driven by the $\pi-\pi$ overlap of the disks and the unfavorable interactions between the cores and the alkyl chains leading to phase separation and to self-assemblies at the nanoscale.[2,3] Applications of DLCs as electronic devices rely on the optimal stacking of the aromatic cores that allows for charge carrier mobility along the columnar axis (i.e., molecular wires).[4] In this respect the self-assembly and electronic properties of large aromatic cores such as hexa-*peri*-hexabenzocoronenes (HBC) have been explored extensively.[2−5]

Among the different DLCs, perylenediimide (PDI) derivatives have received considerable attention originally because of their industrial applications as pigments.[6,7] Efforts to optimize pigment colors resulted in high grade industrial applications including automotive coatings. These applications made use of the high tinctorial strength, light and weather stability, insolubility, and chemical inertness of PDIs. Other major applications of PDI derivatives are as organic electronics in all-organic photovoltaic solar cells[8,9] and field-effect transistors.[10] These applications rely on the high charge carrier mobilities that made PDI the best n-type semiconductors available to date.[11] In addition, the recently synthesized perylenemonoimide (PMI)[12−14] and diimide dyes are widely used as chromophores in fluorescence experiments[15] and for single molecule spectroscopy.[16] Central to these applications of HBCs and PDIs is their ability

---

[†] University of Ioannina and FORTH-BRI.

[‡] Max-Planck Institute for Polymer Research.

(1) *Handbook of Liquid Crystals*; Demus, D., Goodby, J., Gray, G. W., Spiess, H.-W., Vill, V., Eds.; Wiley-VCH: Weinheim, 1998.

(2) Wu, J.; Pisula, W.; Müllen, K. *Chem. Rev.* **2007**, *107*, 718–747.

(3) Schmidt-Mende, L.; Fechtenkötter, A.; Müllen, K.; Moons, E.; Friend, R. H.; MacKenzie, J. D. *Science* **2001**, *293*, 1119–1122.

(4) Feng, X.; Marcon, V.; Pisula, W.; Hansen, M. R.; Kirkpatrick, J.; Grozema, F.; Andrienko, D.; Kremer, K.; Müllen, K. *Nat. Mater.* **2009**, *8*, 421–426.

(5) Pisula, W.; Menon, A.; Stepputat, M.; Lieberwirth, I.; Kolb, U.; Tracz, A.; Sirringhaus, H.; Pakula, T.; Müllen, K. *Adv. Mater.* **2005**, *17*, 684–689.

(6) Herbst, W.; Hunger, K. *Industrial Organic Pigments: Production, Properties, Applications*, 2nd ed.; Wiley-VCH: Weinheim, 1997.

(7) Würthner, F. *Chem. Commun.* **2004**, *14*, 1564–1579.

(8) Schmidt-Mende, L.; Fechtenkotter, A.; Müllen, K.; Moons, E.; Friend, R. H.; MacKenzie, J. *Science* **2001**, *293*, 1119–1122.

(9) Tang, C. W. *Appl. Phys. Lett.* **1986**, *48*, 183–185.

(10) Gsänger, M.; Oh, H.; Könemann, M.; Höffken, H. W.; Krause, A.-M.; Bao, Z.; Würthner, F. *Angew. Chem., Int. Ed.* **2010**, *49*, 740–743.

(11) Dimitrakopoulos, C. D.; Malenfant, P. R. L. *Adv. Mater.* **2002**, *14*, 99–117. Avlasevich, Y.; Li, C.; Müllen, K. *J. Mater. Chem.* **2010**, *20*, 3814–3826, and references therein.

(12) Li, C.; Schoeneboom, J.; Liu, Z.; Pschirer, N. G.; Erk, P.; Herrmann, A.; Müllen, K. *Chem.*−*Eur. J.* **2009**, *15*, 878–884.

(13) Edvinsson, T.; Li, C.; Pschirer, N.; Schoeneboom, J.; Eickemeyer, F.; Sens, R.; Boschloo, G.; Herrmann, A.; Müllen, K.; Hagfeldt, A. *J.Phys. Chem. C* **2007**, *111*, 15137–15140.

(14) Li, C.; Liu, Z.; Schoeneboom, J.; Eickemeyer, F.; Pschirer, N. G.; Erk, P.; Herrmann, A.; Müllen, K. *J. Mater. Chem.* **2009**, *19*, 5405–5415.

(15) Koynov, K.; Mihov, G.; Mondeshki, M.; Moon, C.; Spiess, H. W.; Müllen, K.; Butt, H.-J.; Floudas, G. *Biomacromolecules* **2007**, *8*, 1745–1750.

(16) Wöll, D.; Braeken, E.; Deres, A.; De Schryver, F. C.; Uji-i, H.; Hofkens, J. *Chem. Soc. Rev.* **2009**, *38*, 313–328.

10.1021/ja102150g © 2010 American Chemical Society

Scheme 1. Schematic of the Five PMI Derivatives Investigated

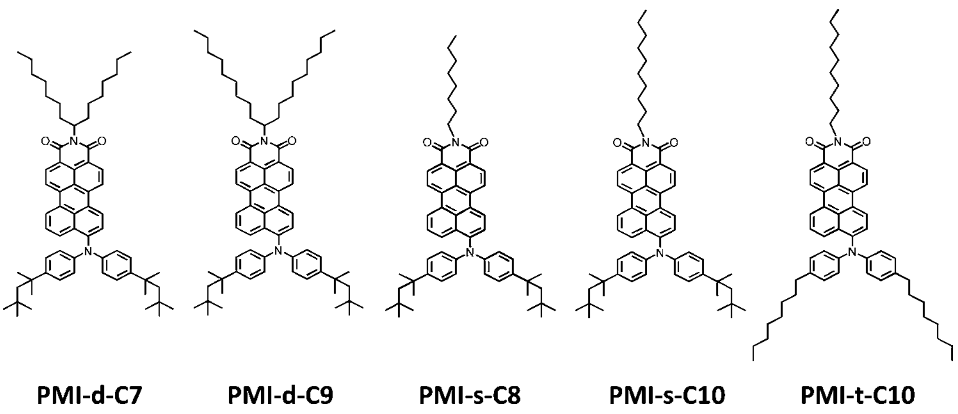

to organize efficiently in different packing motifs and in particular their degree of intra- and intermolecular order. The degree of structural perfection strongly affects their molecular properties (absorbance, fluorescence, and charge transport) and results in applications in organic field-effect transistors, light-emitting diodes, and organic solar cells.

Several reports exist on the thermotropic liquid crystalline behavior of symmetrically[17,18] and, more recently, asymmetrically[19] substituted PDIs, but none exist on the slow molecular dynamics that include the cooperative disk rearrangements, which are coupled to the stability of columns.[20] The influence of self-assembly on the charge carrier mobility of PDI derivatives revealed a helical molecular arrangement with a 45° twist angle between successive molecules.[21] However, the optimal alignment for electron transport was found to be either cofacial or twisted by 65°.[4] When the local molecular order was investigated by solid-state NMR spectroscopy,[22] the twist angle was in the range of 20−40° and the molecular motion in the core was practically frozen. By substituting the same PDI core with tri(ethylene glycol) chains the twist angle increased to 90°.[23] Furthermore, the influence of core extension (e.g., terrylenediimides and quaterrylenediimides) on the thermotropic behavior of PDI was studied[18] and revealed a helical stacking of disks with a lateral rotation of 45°. These examples illustrate the importance of the core and chain substitution in controlling both the phase behavior and the molecular stacking within the columns.

Despite the important knowledge on controlling the self-assembly of perylenes, little is known on how molecular motion is related to the phase state and in turn how the dynamics are coupled to the stability and possibly the self-healing properties of the columnar assemblies. Prerequisites for the dynamic investigations are a strong molecular dipole and nearby specific heteronuclear sites that can be probed independently by dielectric spectroscopy and site-specific NMR spectroscopies, respectively. The donor−acceptor character of the substituted perylene core makes PMIs ideal systems for investigating the molecular dynamics within the different phases. On the other hand, the symmetric core of HBCs requires additional dipole functionalization. Recent work[24] on dipole-functionalized HBCs revealed fast and slower molecular dynamics associated, respectively, with the disk axial motion and with a collective reorganization of the columns that completely relaxes the dipole moment. These studies also provided the first phase diagrams[25] for HBCs and highlighted the importance of metastable states toward the final equilibrium structures.[26]

The present work relies on the strong dipole associated with the donor−acceptor character of the molecules. It explores the role of alkyl chain substitution on (i) the phase formation and (ii) the slow core dynamics in diphenylamine functionalized PMIs. Five PMIs with alkyl chains substitution were investigated (Scheme 1), and their self-assembly was found to depend strongly on the space-filling properties of the branched alkyl chains rather than the mere number of linear alkyl chains. Subsequently, we investigated the core dynamics by employing two measures, the large dipole moment of the core, using dielectric spectroscopy (DS), and the heteronuclear dipole−dipole couplings using site-specific solid-state NMR. These probes provide, for the first time, the rate of disk motion together with the geometry of motion within the isotropic and ordered phases of PMIs. The results on the self-assembly and dynamics are compared with the symmetric cores of HBCs. In the last part, we explore the kinetic pathways for the formation of the ordered crystalline phase from the isotropic phase. This study emphasizes the importance of nucleation barriers that lead to the highly ordered helical packing found in perylene derivatives.

Results and Discussion

Self-Assembly. The thermodynamic and structural features of the perylene derivatives are summarized in Table 1. Figure 1 gives the DSC trace of the PMI-d-C9 compound; the traces of

---

(17) Cormier, R. A.; Gregg, B. A. *Chem. Mater.* **1998**, *10*, 1309–1319.
(18) Nolde, F.; Pisula, W.; Müller, S.; Kohl, C.; Müllen, K. *Chem. Mater.* **2006**, *18*, 3715–3725.
(19) Wicklein, A.; Lang, A.; Muth, M.; Thelakkat, M. *J. Am. Chem. Soc.* **2009**, *131*, 14442–14453.
(20) Percec, V.; Glodde, M.; Bera, T. K.; Miura, Y.; Shiyanovskaya, I.; Singer, K. D.; Balagurusamy, V. S. K.; Heiney, P. A.; Schnell, I.; Rapp, A.; Spiess, H. W.; Hudson, S. D.; Duan, H. *Nature* **2002**, *419*, 384–387.
(21) Marcon, V.; Breiby, D. W.; Pisula, W.; Dahl, J.; Kirkpatrick, J.; Patwardhan, S.; Grozema, F.; Andrienko, D. *J. Am. Chem. Soc.* **2009**, *131*, 11426–11432.
(22) Hansen, M. R.; Graf, R.; Sekharan, S.; Sebastiani, D. *J. Am. Chem. Soc.* **2009**, *131*, 5251–5256.
(23) Hansen, M. R.; Schnitzler, T.; Pisula, W.; Graf, R.; Müllen, K.; Spiess, H. W. *Angew. Chem., Int. Ed.* **2009**, *48*, 4621–4624.
(24) Elmahdy, M. M.; Floudas, G.; Mondeshki, M.; Spiess, H. W.; Dou, X.; Müllen, K. *Phys. Rev. Lett.* **2008**, *100*, 107801–107804.
(25) Elmahdy, M. M.; Dou, X.; Mondeshki, M.; Floudas, G.; Butt, H.-J.; Spiess, H. W.; Müllen, K. *J. Am. Chem. Soc.* **2008**, *130*, 5311–5319.
(26) Elmahdy, M. M.; Mondeshki, M.; Dou, X.; Butt, H.-J.; Spiess, H. W.; Müllen, K.; Floudas, G. *J. Chem. Phys.* **2009**, *131*, 114704–114709.

Table 1. Thermal Properties, Transition Temperatures, and Structural Details

sample	transition temp (K)	enthalpy (J/g)	phase/phase transition	d_{10} (nm)^d	d_{01} (nm)^d	d_{intra} (nm)^d
PMI-d-C9	468^a $(451)^b$ $-^c$	20.6^a $(19.8)^b$	Cr-I/glass temp	2.054	1.188	0.350
PMI-d-C7	500^a	23.9^a	Cr-I	1.916	1.114	0.350
PMI-s-C8	346^a $(347)^b$ 352^c		I/glass temp			
PMI-s-C10	338^a $(327)^b$ 344^c		I/glass temp			
PMI-t-C10	281^a $(274)^b$ 291^c		I/glass temp			

^{a} Heating (differential scanning calorimetry). ^{b} Cooling (differential scanning calorimetry). ^{c} Cooling (dielectric spectroscopy). Col$_h$: columnar hexagonal liquid crystalline phase. Cr: crystalline phase. I: isotropic. ^{d} At 303 K.

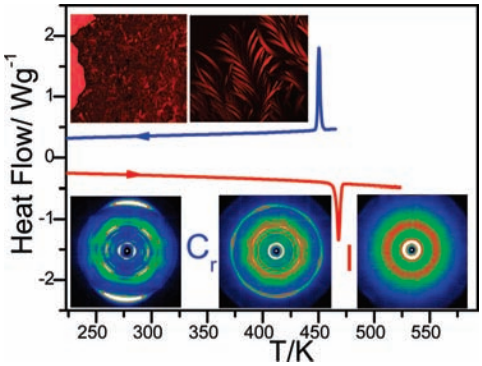

Figure 1. DSC trace of the PMI-d-C9 compound obtained on cooling (blue) and subsequent heating (red) at 10 K/min. (Top) Two POM images obtained on cooling at 448 and 464 K depicting spherulites and dendritic textures, respectively. (Bottom) 2D WAXS structures from oriented fibers obtained on heating at 303, 453, and 478 K. The images at 303 and 453 K correspond to the Cr phase, whereas the one at 478 corresponds to the isotropic phase (I).

the remaining compounds are given in Figure S1in Supporting Information. With the exception of PMI-d-C9 and PMI-d-C7, all perylene derivatives undergo an isotropic liquid-to-glass transformation at different temperatures that depends on the number of methylene units. On the other hand, PMI-d-C9 undergoes an isotropic (I) to crystalline (Cr) transition at 468/451 K (heating/cooling) with an associated heat of fusion/crystallization of 20.6/19.8 J/g. PMI-d-C7 does not undergo any transformation up to the highest temperature investigated. All samples were further investigated with polarizing optical microscopy (POM). As expected, they show an isotropic phase with the exception of PMI-d-C9 and PMI-d-C7 where massive structures were observed under very fast (50 K/min) cooling. Two POM images of the PMI-d-C9 structures obtained on cooling at 448 and 464 K are depicted in Figure 1. The structures observed at low temperatures are spherulitic (with the typical maltese cross) with well-defined boundaries. At higher temperatures the structures resemble more a pseudofocal conical fan shape, with dendritic inner textures showing a 60° branching.

To obtain the required information on the self-assembly at the unit cell level wide-angle X-ray scattering (WAXS) was employed. Three WAXS images of PMI-d-C9 are shown in Figure 1 at 303, 453, and 478 K. The images at 303 and 478 K correspond to the Cr and I phases, respectively, whereas the one at 453 K is in the vicinity of the melting process of the Cr phase. The WAXS image at 303 K, which is typical of the Cr phase, contains a set of equatorial reflections. These correspond to the (10) (01) (11) (20) and (21) reflections from an orthorhombic unit cell that is depicted in Figure 2. The d_{hk} spacings, where h and k are the Miller indices, are related to the lattice parameters a = 1.981 nm, at 333 K and b = 1.200 nm, at 333 K through

$$\frac{1}{d_{hk}^2} = \frac{h^2}{a^2} + \frac{k^2}{b^2} \tag{1}$$

In addition, the image contains two meridional reflections with spacings of 0.35 and 2 nm that reflect intramolecular periodicities. The former is the typical distance found in graphite and corresponds to the intramolecular layer distance in a stacked columnar arrangement of perylenes. The latter spacing (2 nm) being 6 times the layer spacing of 0.35 nm, corresponds to a helical pitch of molecules rotated by 60° (Figure 2). Notice the absence of tilting of molecules within the Cr phase that contrasts to the well-known “herringbone” structure found in the Cr phase of some discotic liquid crystals. Herein the elongated shape of the core minimizes the $\pi-\pi$ overlap and prevents tilting.

Figure 3 gives the temperature dependence of the lattice parameters a, b, and c of the orthorhombic unit cell and of the unit cell volume ($V = abc$) for both PMI-d-C9 and PMI-d-C7. The longer alkyl chains in the former result in an expanded orthorhombic unit cell; however, the intradisk periodicities are identical. The respective coefficients of thermal expansion ($a_a = (\partial \ln a/\partial T)_P$), for PMI-d-C9 amount to a_a=1.776 × 10^{-4} K^{-1}, a_b=1.811 × 10^{-4} K^{-1}, and a_c=1.069 × 10^{-4} K^{-1}, whereas the volumetric thermal expansion coefficient amounts to $\beta = 4.656 \times 10^{-4}$ K^{-1}. Notice that all values are positive, in contrast to the Cr phase in HBCs, where a volume contraction (i.e., negative thermal expansion) was found to result from the increasing tilting of the HBC cores within the columns of the Cr phase.[27] Furthermore, $a_a \approx a_c$, i.e., intra- and intercolumnar thermal expansions are nearly isotropic, in contrast to the symmetric cores of triphenylenes and HBCs.[27] Again the anisotropic donor−acceptor character of the core that minimizes the $\pi-\pi$ interactions and promotes the helical stacking of perylene molecules within the columns is responsible for the more isotropic thermodynamic properties.

Additional insights into the columnar packing of PMI-d-C9 molecules observed in the WAXS experiments (see above) can be obtained from solid-state NMR spectroscopy. As we have recently shown, the ^{1}H NMR chemical shifts of the PDI core protons represents a sensitive probe with respect to the specific pitch-angle between successive molecules.[22] Moreover, that study utilized branched alkyl side chains, though symmetrically attached and slightly shorter (i.e., PDI-C8,7 the molecular structure is depicted in Supporting Information as Scheme S1), as in the present case of PMI-d-C9. It was also observed that for low pitch angles (α < 25°), an intense autocorrelation signal originating from the branching CH moieties of the side chains is to be expected in the 2D ^{1}H−^{1}H double-quantum (DQ) single-quantum (SQ) correlation spectrum.[22] This was later explained with respect to the morphology of the sample using MD

---

(27) Grigoriadis, C.; Haase, N.; Butt, H.-J.; Müllen, K.; Floudas, G. *Adv. Mater.* **2010**, *22*, 1403–1406.

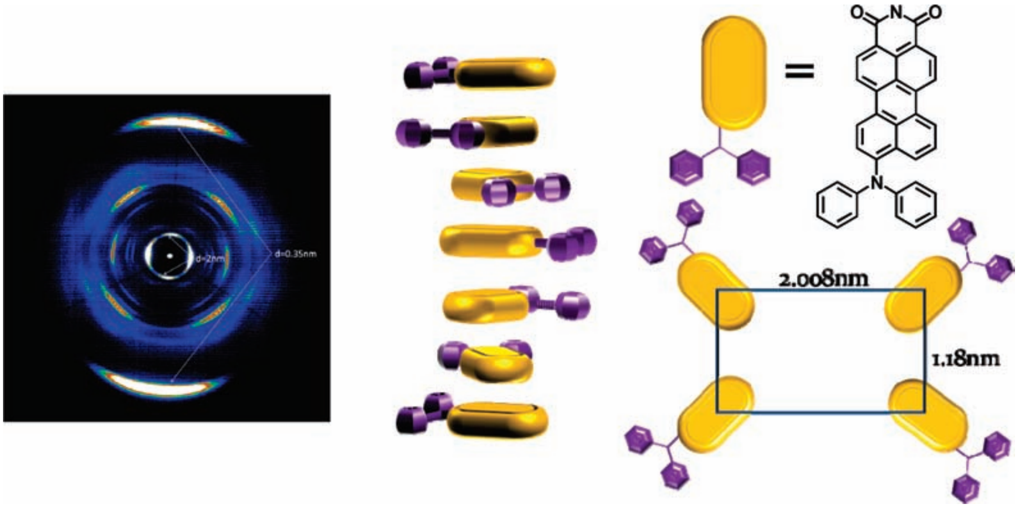

Figure 2. Graphical representation of the PMI-d-C9 orthorhombic unit cell (right), extracted from WAXS. The representation on the left depicts a helical arrangement of 7 units with a successive rotational angle of 60° that is based on the WAXS study.

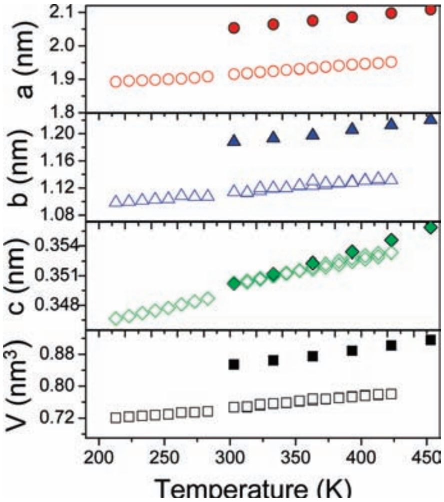

Figure 3. Temperature dependence of the orthorhombic unit cell parameters (*a*, *b*, and *c*) and of the corresponding volume, *V*, of PMI-d-C9 (filled symbols) and PMI-d-C7 (open symbols).

simulations by Marcon et al.[21] In Figure 4a the spatial proximity of protons in PMI-d-C9 is mapped out using the before-mentioned NMR technique for a fast spinning frequency of 50.0 kHz. From this spectrum it is evident that the region corresponding to the PMI core protons overlaps with those of the phenyls in the diphenylamines chains even at this high spinning frequency. However, taking into account that the PMI core protons are shifted to high field as a result of $\pi-\pi$ interactions,[28−31] it is possible to perform the assignment as illustrated in Figure 4a. More importantly, the spectrum shown in Figure 4a does not reveal any autocorrelation signal between the branched C9 side chains of neighboring molecules. This constitutes a clear evidence that the PMI-d-C9 molecules are packed in columnar stacks with an angle between successive molecules larger than 30°. Taking into account that the pairwise signals observed for the PDI core protons show a splitting of ~0.8 ppm (cf. Figure 5 in ref 22), the pitch angle is estimated to be in the range of 50−70°. This is in full agreement with the assignment based on the WAXS investigation.

To relate the observed ^{1}H chemical shifts in Figure 4a to their specific carbon sites in PMI-d-C9, a 2D ^{13}C{^{1}H} FSLG-HETCOR experiment has been performed as depicted in Figure 4c. Here, the experiment is conducted at a significantly lower spinning frequency ($\upsilon_R = 15.0$ kHz) compared to that of Figure 4a, and in order to achieve the same resolution in the ^{1}H dimension, a frequency-switched Lee−Goldburg (FSLG) sequence has been employed.[32,33] In the aromatic region (110−130 ppm) all ^{13}C resonances can be assigned to their directly attached ^{1}H, whereas the assignment in the aliphatic region is less straightforward. Interestingly, the peak corresponding to the branching proton of the C9,9 side chain (CH moiety) is split into two signals, i.e., pairs of signals at 1.7 and 58 ppm and 4.8 and 54 ppm for ^{1}H and ^{13}C, respectively, can be observed. The existence of two distinct signals for the branching proton illustrates that two conformations of the C9,9 side chains coexist, namely, one that is hydrogen bonded ($\delta_{\mathrm{iso}}(^1\mathrm{H}) \approx 4.8$ ppm) and thereby coordinated to one of the carbonyls of either side of the PMI core, and a second conformation, where the proton ($\delta_{\mathrm{iso}}(^1\mathrm{H}) \approx 1.7$ ppm) is non-hydrogen-bonded. We note that this kind of splitting was not observed for PDIs with symmetrically attached C8,7-branching moieties with alkyl and tri(ethylene glycol) substituents.[22,23] In these systems only the hydrogen-bonded fractions were detected. To investigate the stability of the hydrogen-bonded species in PMI-d-C9, a series of temperature-dependent ^{13}C{^{1}H} CP/MAS NMR experiments have been performed as illustrated in Figure 5a. It can readily be seen that the two different side-chain conformations persist in the measured temperature range and that the isotropic ^{13}C chemical shift for both fractions is slightly shifted toward lower fields with increasing temperature. Moreover, the ^{13}C resonance corresponding to the non-hydrogen-bonded fraction (~58.5 ppm) becomes narrower, whereas the resonance for the hydrogen-

---

(28) Ochsenfeld, C.; Brown, S.; Schnell, I.; Gauss, J.; Spiess, H. W. *J. Am. Chem. Soc.* **2001**, *123*, 2597–2606.

(29) Brown, S. P.; Spiess, H. W. *Chem. Rev.* **2001**, *101*, 4125–4155.

(30) Brown, S. P. *Prog. Nucl. Magn. Reson. Spectrosc.* **2007**, *50*, 199–251.

(31) Brown, S. P. *Macromol. Rapid Commun.* **2009**, *30*, 688–716.

(32) Bielecki, A.; Kolbert, A.; Levitt, M. *Chem. Phys. Lett.* **1989**, *155*, 341–346.

(33) van Rossum, B. J.; Förster, H.; de Groot, H. J. M. *J. Magn. Reson.* **1997**, *124*, 516–519.

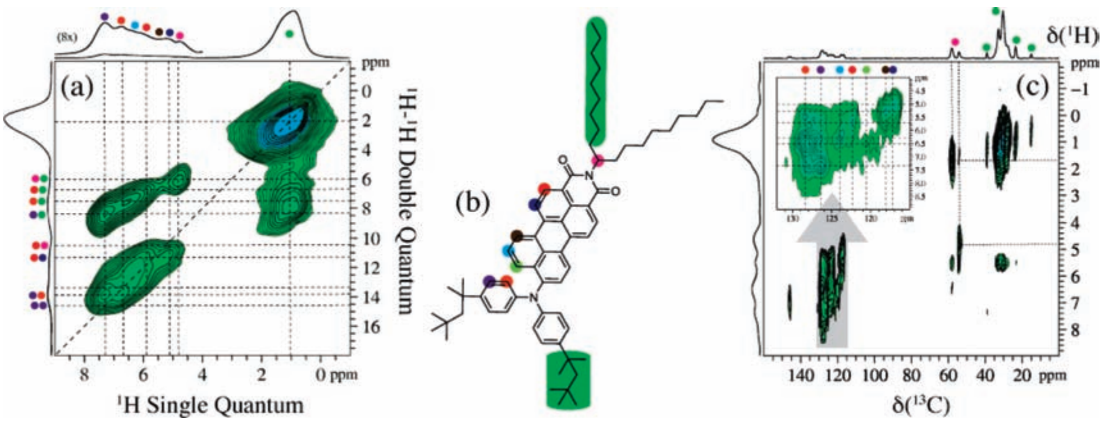

Figure 4. (a) 2D rotor-synchronized $^{1}H-^{1}H$ DQ-SQ correlation spectrum of PMI-d-C9 recorded using a spinning frequency of 50.0 kHz and a BaBa DQ excitation/reconversion period of 40 μs ($2\tau_R$). (b) Molecular structure of PMI-d-C9 including the color scheme employed for assignment purposes in this work. (c) 2D $^{13}C\{^{1}H\}$ FSLG-HETCOR spectrum of PMI-d-C9 recorded using a spinning frequency of 15.0 kHz for a short cross-polarization period of 500 μs. The inset in panel c corresponds to an expansion of the region marked by the gray arrow. In panels a and c the dashed lines indicate the internuclear contacts and directly bonded protons to carbons, respectively.

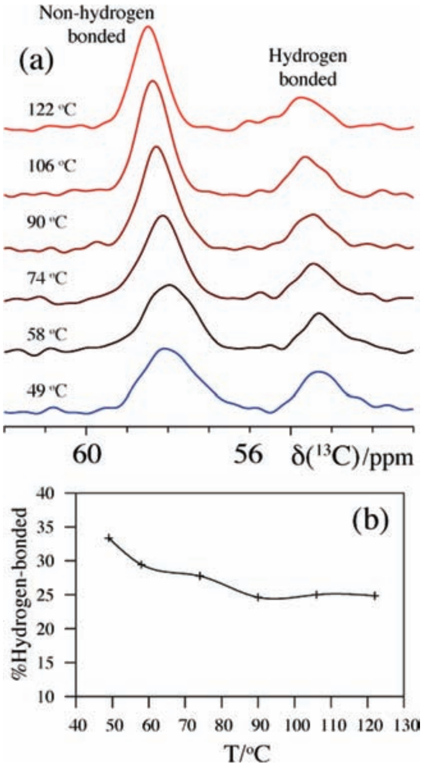

Figure 5. (a) Variable-temperature $^{13}C\{^{1}H\}$ CP/MAS NMR spectra acquired using a spinning speed of 25.0 kHz and a cross-polarization time of 500 μs. The selected region shows how the ratio between hydrogen-bonded and non-hydrogen-bonded changes upon heating the samples to higher temperatures (below melting point). (b) Illustration of how the fraction of hydrogen-bonded species drops as a function of temperature. The solid line connecting the data points corresponds to an approximated spline and is meant as a guide for the eye only.

bonded (~54.5 ppm) remains broad. An integration of the peak intensities shows that the fraction of hydrogen-bonded protons decreases with increasing temperature as depicted in Figure 5b. These observations indicate that the non-hydrogen-bonded fraction is more mobile than the hydrogen-bonded fraction, whose mobility appears to be unaffected by temperature.

The fact that two side-chain conformations coexist in PMI-d-C9 with a pitch angle of 60°, whereas solely hydrogen-bonded conformations were found in PDI-C8,7, where the pitch angle is in the range of 20−45°, is suggestive of a relation between the helical intracolumnar organization of the cores and the space-filling requirements of the side chains.[21,22] The presence of hydrogen-bonded conformations (as in PDI-C8,7) drives the alkyl chains to orient perpendicular to the perylene core, allowing for a smaller pitch angle. On the other hand, the presence of a fraction of non-hydrogen-bonded conformations drives a number of branched side chains away from the perpendicular orientation, and this may twist the cores to larger angles to preserve a uniform density within the alkyl domains. In particular, it has already been pointed out in 1983[34] that the columnar mesophase, as realized by rigid aromatic core molecules and more flexible aliphatic side chains, poses packing problems because of the incommensurability of the aliphatic and aromatic moieties. This packing question is particularly important in cases of elongated cores, where density modulations as proposed by de Gennes[34] were indeed observed.[35,36] Therefore, the question of whether such systems can crystallize is particularly intriguing.

To draw quantitative conclusions on the rigidity of the PMI-d-C9 core and on the expected difference in mobility between hydrogen-bonded and non-bonded branching protons of the C9,9 side chain, we have recorded a series of site-specific heteronuclear rotor-encoded dipolar sideband patterns, using the rotor-encoded polarization transfer (REPT-HDOR) technique.[37] In this kind of experiment, the local molecular motion is monitored through the effective $^{1}H-^{13}C$ dipole−dipole coupling (D_{CH}), corresponding to the time-averaged value of the anisotropic heteronuclear dipolar Hamiltonian, which spatial part is described by a second-order Legendre polynomial. The measured dipole−dipole couplings can be related to an effective order parameter using the dipole−dipole coupling constant for a static $^{1}H-^{13}C$ spin pair of 21.0 kHz,[37] using the relation

---

(34) de Gennes, P.G. J. *Phys. Lett.* **1983**, *44*, 657–664.
(35) Werth, M.; Leisen, J.; Boeffel, C.; Dong, R. Y.; Spiess, H. W. *J. Phys. II* **1993**, *3*, 53–67.
(36) Hollander, A.; Hommels, J.; Prins, K. O.; Spiess, H. W.; Werth, M. *J. Phys. II* **1996**, *6*, 1727–1741.
(37) Saalwachter, K.; Schnell, I. *Solid State Nucl. Magn. Reson.* **2002**, *22*, 154–187.

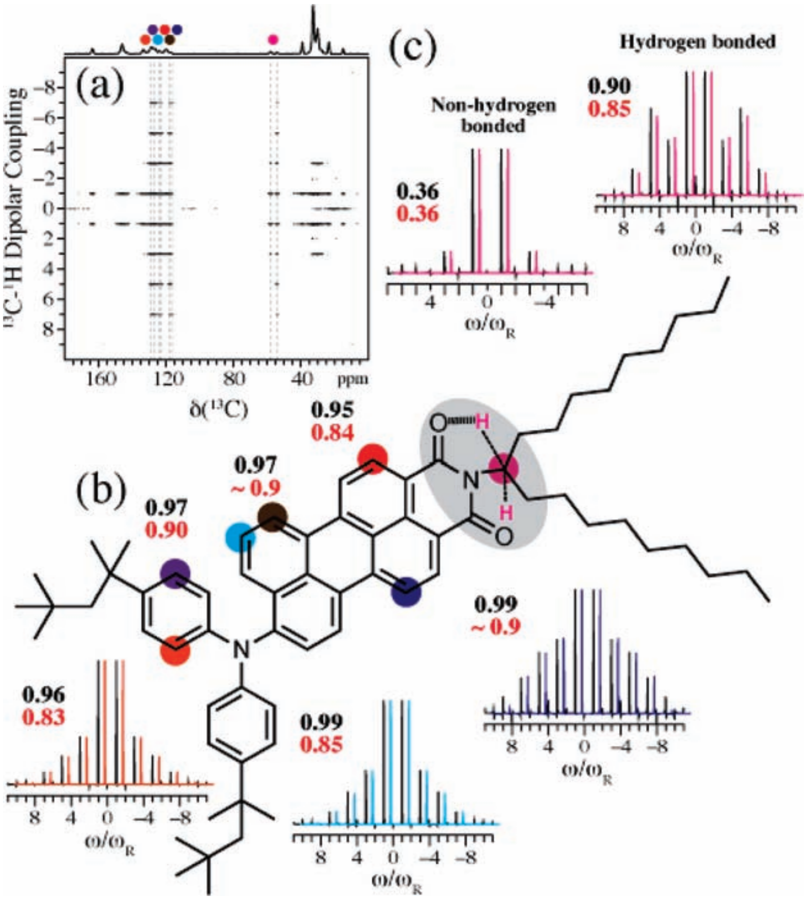

Figure 6. (a) 2D contour plot of the ^{13}C{^{1}H} REPT-HDOR spectrum for PMI-d-C9 recorded at ambient conditions for a spinning speed of 30.0 kHz and a recoupling period of 134.4 μs (4τ_R). The site-selective ^{13}C−^{1}H dipolar sideband patterns shown in black in panels b and c have been extracted from the positions indicated in panel a by dashed lines. The optimized simulations are shown in colors (see Figure 1b) and have been slightly shifted to the right for a better visual comparison with their experimental contour parts. The upper numbers (black) and lower numbers (red) given in bold correspond to the dynamic order parameters (eq 2) determined at ambient temperature and 122 °C, respectively.

$$S = \left\langle \frac{1}{2}(3\cos^2\theta_{CH}(t) - 1) \right\rangle = \frac{\langle D_{CH}(t)\rangle_t}{D_{CH,static}} \qquad (2)$$

The results from this investigation are shown in Figure 6 at ambient temperature and at an elevated temperature of 122 °C but below the melting point. Clearly, at ambient temperature the measured effective order parameters show that PMI-d-C9 is crystalline and that its core hardly moves within the columns on the time scale of the NMR experiment. This freezing of molecular dynamics is expected to have consequences on the dynamics of the core as probed by dielectric spectroscopy (see below). Furthermore, the two C9,9 branching points show vastly different local dynamics with $S_{H\text{-bonded}} \approx 0.9$ and $S_{non\text{-H-bonded}} \approx 0.4$, as anticipated from the variable-temperature ^{13}C{^{1}H} CP/MAS NMR experiments. It seems that *mobile* non-hydrogen-bonded branched alkyl chain conformations are required to fill the space and produce a uniform density. At 122 °C the effective order parameters are slightly lowered, indicating that the cores of the PMI-d-C9 stacked molecules are slightly fluctuating. The effective order parameters for the two different side-chain conformations are affected in a similar manner.

Summarizing, the structural investigation revealed that the self-assembly and thermodynamic properties of perylene derivatives are distinctly different from those of the corresponding HBC compounds. Although both form columnar phases, the self-assembly within the columnar stacks differs substantially. Perylenes, with a small $\pi-\pi$ overlap, do form a crystalline phase as well, but the molecules do not tilt with respect to the columnar axis. Because of this, the intercolumnar thermal expansion is always positive, being similar to the intracolumnar thermal expansion. This constitutes the primary difference in the self-assembly motifs of the Cr phase of perylenes as compared to HBCs. They do share, however, some similarities. As observed for HBCs, phase formation involves a delicate balance of short-ranged interactions and packing. From the different perylene derivatives investigated, only the PMI-d-C7 and PMI-d-C9 derivatives crystallize, whereas the structurally similar PMI-s-C10 and PMI-t-C10 compounds do not. The fact that the PMI-t-C10 does not crystallize is, at first sight, surprising given the presence of three long alkyl chains. The absence of crystallization in PMI-s-C10 suggests that chain length alone is not the rate-determining factor for the formation of the Cr phase. In view of recent work[19,21−23] on other swallow-tail substituted perylenes and the present results, it is likely that branched chains substituted away from bay positions are required as space-filling agents for the formation of the more ordered Cr phase. These chains are most effective as they lessen the packing problems discussed earlier.[34] The solid-state NMR experiments further pointed out the importance of hydrogen bonding in stabilizing the crystalline phase. Within the columnar stacks of the Cr phase, PMI molecules had a helical arrangement with a pitch of 2 nm, corresponding to a 60° rotation of successive molecules.

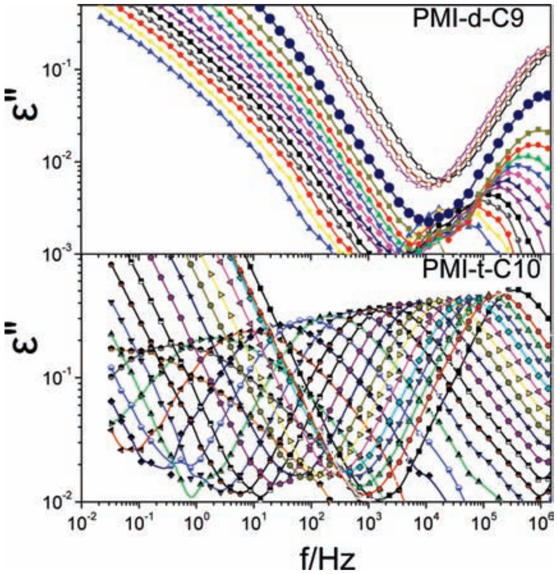

Figure 7. Dielectric loss spectra of PMI-d-C9 (top) and of PMI-t-C10 (bottom) shown at different temperatures: $398 \leq T \leq 473$ K and $293 \leq T \leq 393$ K, respectively, in 5 K steps. Notice the reduction in the dielectric loss of PER-d-C9 at 458 K (shown with the thick solid circles) that is absent in PMI-t-C10.

Within the Cr phase the molecular dynamics are restricted as indicated by the NMR local order parameters, and this is expected to show up in the dynamic studies (see below).

Molecular Dynamics. The molecular dynamics were subsequently investigated with dielectric spectroscopy. Figure 7 provides the measured dielectric loss curves for PMI-d-C9 in comparison to PMI-t-C10. The dielectric response of PMI-d-C9, which undergoes an I-to-Cr transition, is distinctly different from that of the remaining compounds. A strong single peak, albeit broad, is seen in PMI-t-C10 as well as in PMI-s-C8, PMI-s-C10, and PMI-t-C10, arising from the reorientation within the I phase. With decreasing temperature the process freezes out at the liquid-to-glass temperature, defined here as the temperature where the corresponding relaxation time is at $\tau \approx 100$ s. The single dynamic process in PMI-t-C10 clearly violates the time−temperature superposition principle (not shown here) as a result of the T-dependent distribution of relaxation times. Figure 8 provides the temperature-dependence of the low frequency Havriliak−Negami parameter (m) (eq S1, Supporting Information) associated with longer range dynamics. At $T \gg T_g$ the shape parameter resembles a Debye process. With decreasing temperature the distribution of relaxation times broadens and for PMI-t-C10 attains a value of $m \approx 0.5$ at $T = T_g$. On the other hand, the erratic $m(T)$ for PMI-d-C9 reflects the loss of dielectric strength on entering the Cr phase (see below).

Crystallization has profound consequences on the dipolar relaxation of PMI-d-C9 and PMI-d-C7. In PMI-d-C7 crystallization is so strong that it suppresses any dielectric activity. On the other hand, in PMI-d-C9 and at temperatures corresponding to the I phase, the dielectric loss curves are reminiscent to those of PMI-t-C10 (Figure 7) with typical peak values of $\varepsilon''_{\max} \approx 0.3$. The transition to the Cr phase is accompanied by a discontinuous reduction of the dielectric strength of both the peak and the ionic conductivity and by peak broadening. The reduced dielectric strength is suggestive of a restricted dipole reorientation within the Cr phase, in agreement with the high values of the dynamic order parameter found in NMR ($S \approx 0.9-0.95$). In addition to the dynamics, the dielectric strength $\Delta\varepsilon$ ($= \varepsilon_S' - \varepsilon_\infty'$, where $\varepsilon_S' = \lim_{\omega\to 0} \varepsilon'(\omega)$ and $\varepsilon_\infty' = \lim_{\omega\to\infty} \varepsilon'(\omega)$), together with the molecular dipole moment allows an estimation of the angle between interacting perylene molecules within the column through[38]

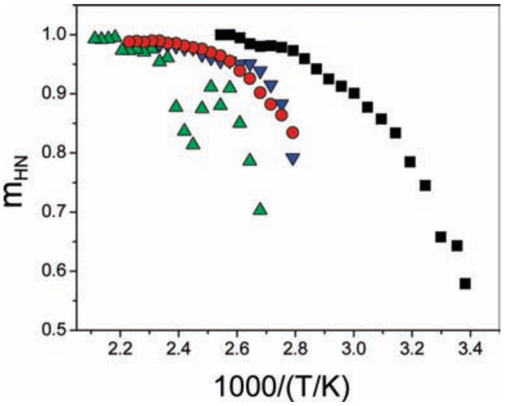

Figure 8. Temperature dependence of the low-frequency HN shape parameter for the four perylene compounds: (■) PMI-t-C10, (▲) PMI-d-C9, (●) PMI-s-C8, and (▼) PMI-s-C10.

$$\Delta\varepsilon \approx \frac{\mu^2}{3k_B T} F g \frac{N}{V} \tag{3}$$

In eq 3, μ is the dipole moment for noninteracting dipoles, F [$= (\varepsilon_S(\varepsilon_\infty + 2)^2/3(2\varepsilon_S + \varepsilon_\infty)$] is the local field correction, g is the Kirkwood−Fröhlich correlation factor giving the angular correlations between the dipoles (approximated by $g = 1 + z\langle\cos \varphi\rangle$, where z is the coordination number or number of closest/interacting neighbors and φ is the angle between the test dipole and its nearest neighbor), N is the number of dipoles, and V is the volume. In the calculation we have assumed intracolumnar dipole−dipole interactions and used the density of the rectangular unit cell ($\rho = 1948.8$ kg/m^3). As for the dipole moment of isolated dipoles we have used the value of 9.7 D (using MOPAC2007). The result for the angle between interacting dipoles within a single column is plotted in Figure S2 in Supporting Information. While the value of the dipole moment has negligible effect on the angle between successive dipoles, the number of interacting dipoles has a significant effect. The estimated angle is higher than the one obtained from WAXS; however, there are several assumptions that are involved in the calculation.

The relaxation times of the four perylene derivatives are summarized in Figure 9. The relaxation times exhibit a strong non-Arrhenius temperature-dependence that conforms to the Vogel−Fulcher−Tammann (VFT) equation:

$$\tau = \tau_0 \exp\left(\frac{B}{T - T_0}\right) \tag{4}$$

where τ_0 is the characteristic time in the limit at very high temperatures, B is the activation parameter, and T_0 is the "ideal" glass temperature (the VFT parameters are summarized in Table 2). In the case of PMI-d-C9, however, the relaxation times display a weaker temperature-dependence that can be described

---

[38] *Broadband Dieletcric Spectroscopy*; Kremer, F., Schönhals, A., Eds.; Springer: Berlin, 2002.

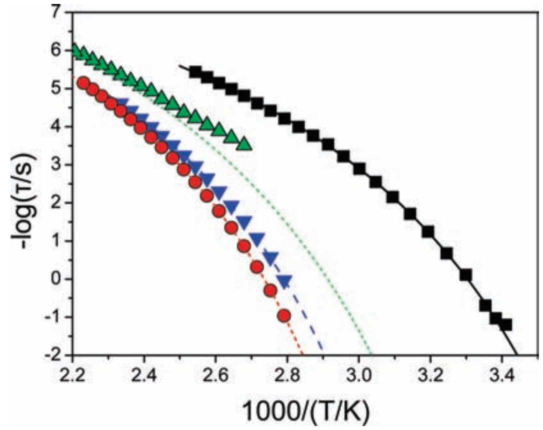

Figure 9. Temperature dependence of the relaxation times extracted from DS for the four perylene compounds: (■) PMI-t-C10, (▲) PMI-d-C9, (●) PMI-s-C8, and (▼) PMI-s-C10. Lines are best fits to the VFT equation except for PMI-d-C9, where a fixed value of the activation parameter corresponding to the I phase was employed instead.

Table 2. Parameters of the VFT Equation

sample	τ_0 (s)	B (K)	T_0 (K)	T_g (K)[b]
PMI-d-C9	$(2.5 \pm 0.1) \times 10^{-11}$	2120[a]	255 ± 1	329 ± 1
PMI-s-C8	$(2.7 \pm 0.2) \times 10^{-11}$	2120 ± 20	278.1 ± 0.5	352 ± 1
PMI-s-C10	$(5 \pm 1) \times 10^{-11}$	2040 ± 53	272 ± 1	345 ± 1
PMI-t-C10	$(1.9 \pm 0.3) \times 10^{-10}$	1610 ± 36	231 ± 1	219 ± 1

[a] Held fixed. [b] From DS at $\tau = 100$ s.

by an Arrhenius law. In this case, the green dashed line in Figure 9 is indicative and refers to a VFT-representation of the high temperature relaxation times, corresponding to the I phase (a fixed value for the activation parameter B was employed). On the basis of the $\tau(T)$ dependencies and the glass temperatures extracted from Figure 9 (given in Table 2), it is apparent that the main effect of alkyl substitution is to increase the rate of molecular motion (i.e., decrease the glass temperature).

Kinetics of Phase Transformation. The presence of a highly ordered Cr phase in PMI-d-C9 allows an investigation of the phase transformation kinetics. In this respect there are several issues that require attention. First is the identification of the exact mechanism of crystallization. We mention here that recent investigations[25,26] of the Cr phase formation in HBCs revealed long-lived metastability and a nucleation and growth mechanism with kinetics that were dominated by the nucleation barrier. Furthermore, an intermediate state was found that involved a change in the unit cell prior to crystallization.[26] On the other hand, the minimal $\pi-\pi$ overlap in PMI-d-C9 prevents molecular tilting along the columns of the Cr phase, and this can influence the transformation kinetics. The present study addresses in detail the mechanism of the Cr phase formation in PMIs following quenches from the high temperature isotropic phase. Emphasis is given to the possible nucleation sites, the relative importance of molecular transport as opposed to the nucleation barrier, and the presence of homogeneous versus heterogeneous nucleation.

To address these questions we have performed "isothermal" kinetic experiments with DS on samples heated to an initial temperature of 220 °C, which is well within the I phase, and then quenched to different final temperatures in the range of 185−189 °C. Subsequently, we monitored the evolution of the dielectric permittivity and loss peaks. For each spectrum the Havriliak−Negami equation was employed and the dielectric strength, $\Delta\varepsilon$, the relaxation time, τ, and the low-frequency shape parameter, m, were extracted as a function of the crystallization time. The results from the kinetic experiments are plotted in Figure 10 for the different final crystallization temperatures. The results for the evolution of $T\Delta\varepsilon$ are more pronounced as anticipated by the reduced disk mobility found in NMR. They display a sigmoidal reduction in dielectric strength with a characteristic time that is a function of the crystallization temperature. The crystallization process is accompanied by moderate changes in the shape parameter and the relaxation time (strictly speaking, the I to Cr transformation is not isochronal).

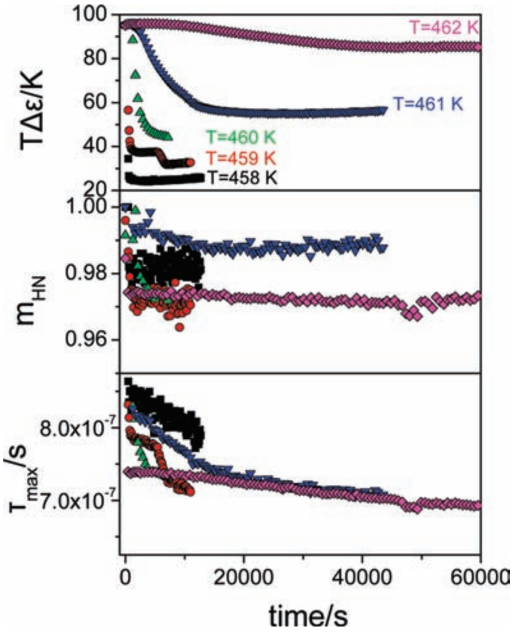

Figure 10. Evolution of the effective dielectric strength ($T\Delta\varepsilon$), low-frequency Havriliak−Negami shape parameter (m), and relaxation time for the PMI-d-C9, following a quench from 493 K to different final crystallization temperatures: (■) 458, (●) 459, (▲) 460, (▼) 461, and (◆) 462 K.

Aiming at the evolution of the volume fraction of the new (Cr) phase we employed a parallel element model (Voigt),[39] which provides an estimate of the crystalline fraction φ_c from

$$\begin{aligned} \varepsilon_S &= \varphi_c \varepsilon_{S,Cr} + (1 - \varphi_c)\varepsilon_{S,I} \\ \varepsilon_\infty &= \varphi_c \varepsilon_{\infty,Cr} + (1 - \varphi_c)\varepsilon_{\infty,I} \\ \Delta\varepsilon(t) &= \varphi_c(t)\Delta\varepsilon_{Cr}(t) + (1 - \varphi_c(t))\Delta\varepsilon_I(t) \end{aligned} \tag{5}$$

the subscripts I and Cr, indicate the isotropic and crystalline phases, respectively. Note that the third equation is obtained by subtraction of the first two. Another lower bound for φ_c can be obtained by assuming additivity of the electric moduli instead, but the resulting equation is more complicated and requires additional parameters. Thus, using eq 5c and the known dielectric strengths of the initial (I) and final (Cr) states we estimate an upper limit for φ_c. The resulting evolution of $\varphi_c(t)$ is plotted in Figure 11 in a double logarithmic representation. The linearity in the latter representation emphasizes that the volume fraction of the Cr phase increases following the well-known Avrami equation:[40]

$$\varphi_c(t) = 1 - \exp(-kt^n) \tag{6}$$

---

(39) Coburn, J. C.; Boyd, R. H. *Macromolecules* **1986**, *19*, 2238–2245.
(40) Avrami, M. J. *J. Chem. Phys.* **1939**, *7*, 1103−1112; **1940**, *8*, 212−224; **1941**, *9*, 177−184.

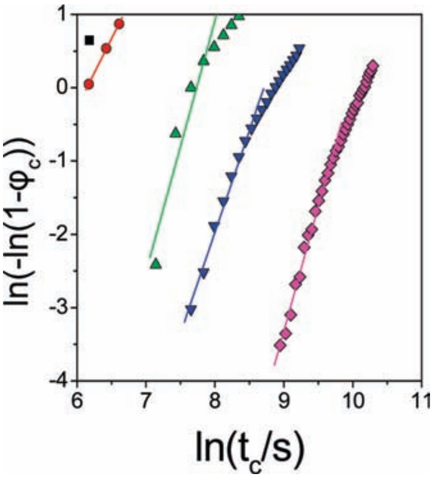

Figure 11. Evolution of the volume fraction φ_c corresponding to the crystalline phase in PMI-d-C9, following a quench from 493 K to different final crystallization temperatures: (■) 458, (●) 459, (▲) 460, (▼) 461, and (◆) 462 K. The lines represent linear fits to the data.

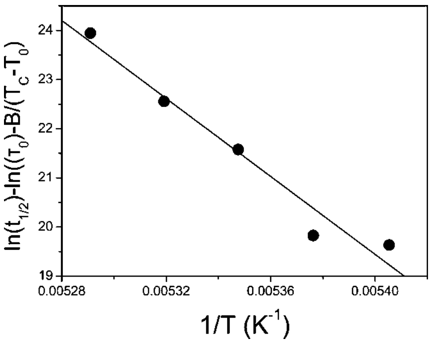

Figure 12. Half-crystallization times in PMI-d-C9 corrected for the diffusion term and plotted as a function of inverse temperature. The slope is proportional to the nucleation barrier (eq 7).

where k and n reflect the rate of transformation and Avrami exponent reflecting the type of nucleation (homogeneous vs heterogeneous) and dimensionality of growth. The n values were in the range of 2−3 for the different temperatures. In a simple nucleation and growth process, the characteristic time, $t_{1/2}$, is a function of the final crystallization temperature, T_c, calculated through $t_{1/2} = (\ln 2/k)^{1/n}$, are related to the nucleation barrier, ΔG^*, through

$$t_{1/2} = \tau_0 \exp\left(\frac{B}{T - T_0}\right) \exp\left(-\frac{\Delta G^*}{k_B T}\right) \qquad (7)$$

The first term in the above equation is the usual mobility term, given by the VFT equation, and the second term is the barrier to crystallization. The latter (ΔG^*) is obtained by plotting $\ln t_{1/2} - \ln \tau_0 - B/(T - T_0)$ vs $1/T$ in Figure 12 and amounts to 3.2 eV. These results show that the kinetics are dominated by the nucleation term.

Other systems with extremely slow relaxation near the phase transition are the spin glasses. In this respect, a random Ising ferromagnetic model with *random* spin predicts slow relaxation and nearly degenerate metastable states.[41,42] The slow dynamics reflect the inability of certain magnetization domains, composed from spins of certain lengths, to spinflip. In particular, the relaxation times grow exponentially with the domain size, L, as $\tau \approx \exp(aL)$. Within this approach, the longer times of transformation found at the higher temperatures reflect simply the larger domain size.

The type of nucleation process can be discussed with respect to the undercooling parameter δ ($= (T_m^o - T_c)/T_m^o$, where T_m^o is the equilibrium melting temperature and T_c is the crystallization temperature) by plotting the characteristic crystallization times as a function of the undercooling for both homogeneous (scales as δ^{-1}) and heterogeneous (δ^{-2}) cases. POM was used to obtain the T_m^o (by following the isothermal crystallization at selected temperatures and by subsequent slow heating to the point that the birefringence disappeared). Within the limited temperature range investigated the nucleation process resembles more closely the homogeneous case.

In summary, the formation of the ordered phase from the isotropic phase proceeds via a nucleation and growth mechanism by overcoming a barrier of 3.2 eV. In addition, the formation of the crystalline phase, despite being very slow at higher temperatures, does not involve any intermediate metastable state.

Conclusions

The first systematic investigation of the self-assembly, the dynamics, and the kinetics of phase formation took advantage of the strong dipole associated with the donor−acceptor character of the diphenylamine functionalized perylenemonoimides molecules and the presence of heteronuclear dipolar couplings. The structural investigation revealed that the self-assembly and thermodynamic properties of perylene derivatives is significantly different from those of the corresponding HBC compounds. Perylenes, with a small $\pi-\pi$ overlap, do form a crystalline phase as well, but the residues do not tilt with respect to the columnar axis. Because of this, the intercolumnar thermal expansion is always positive, being similar to the intracolumnar thermal expansion. This constitutes a primary difference in the self-assembly motifs of the Cr phase of perylenes with the HBCs. Despite this, phase formation involves a delicate balance of short-range interactions and packing. The present results suggest that branched chains substituted away from bay positions are important as space-filling agents within the alkyl domains for the formation of the Cr phase. The results from solid-state NMR experiments further pointed toward the importance of an intramolecular hydrogen bonding in stabilizing the crystalline phase as well as the influence of non-hydrogen-bonded moieties on the twist angle between successive monomers.

With respect to the dynamics, both solid-state NMR and DS revealed a relatively immobile core, characterized by a dynamic order parameters $S \approx 0.9-0.95$, within the crystalline phase of PMI-d-C9. The remaining perylene derivatives that do not crystallize undergo an isotropic liquid-to-glass transformation at a temperature that was found to depend on the number of methylene units in the alkyl chains.

The phase transformation kinetics from the high temperature isotropic phase to the crystalline phase at lower temperatures revealed a long-lived metastable state as a result of the soft potential. The crystalline phase is formed via a nucleation and growth mechanism, and the kinetic times are controlled by the nucleation barriers. The existence of slow molecular dynamics and of very slow kinetics of phase transformation suggests that

---

(41) Takano, H.; Miyashita, S. *Phys. Rev. B* **1993**, *48*, 7221.

(42) Kawasaki, T.; Miyashita, S. *J. Magn. Magn. Mater.* **1992**, *104−107*, 1595. Kawasaki, T.; Miyashita, S. *Prog. Theor. Phys.* **1993**, *89*, 985.

care should be taken in establishing the equilibrium phases of DLC. Furthermore, these issues could influence the charge carrier mobilities that are required for applications as photovoltaic solar cells and field-effect transistors.

Acknowledgment. The current work was supported by the John S. Latsis public benefit Foundation with a research grant to G.F. We thank M. Bach (MPI-P) and G. Tsoumanis (UoI) for technical support. Financial support of the Deutsche Forschungsgemeinschaft, SFB 625 is gratefully acknowledged. M.R.H. acknowledges the Carlsberg Foundation for a Post Doctoral Research Fellowship.

Supporting Information Available: Details on the synthesis, thermal properties, polarizing optical miscopy, X-ray scattering, solid-state NMR spectroscopy, and dielectric spectroscopy. This material is available free of charge via the Internet at http://pubs.acs.org.

JA102150G